

Edge \mathbb{Z}_3 parafermions in fermionic lattices.

Raphael L. R. C. Teixeira¹ and Luis G. G. V. Dias da Silva¹

¹*Instituto de Física, Universidade de São Paulo, C.P. 66318, 05315-970 São Paulo, SP, Brazil*
(Dated: June 12, 2025)

Parafermions modes are non-Abelian anyons which were introduced as \mathbb{Z}_N generalizations of \mathbb{Z}_2 Majorana states. In particular, \mathbb{Z}_3 parafermions can be used to produce Fibonacci anyons, laying a path towards universal topological quantum computation. Due to their fractional nature, much of theoretical work on \mathbb{Z}_3 parafermions has relied on bosonization methods or parafermionic quasi-particles. In this work, we introduce a representation of \mathbb{Z}_3 parafermions in terms of purely fermionic models operators in the t - J regime. We establish the equivalency of a family of lattice fermionic models written in the $t - J$ model basis with a Kitaev-like chain supporting free \mathbb{Z}_3 parafermionic modes at its ends. By using density matrix renormalization group calculations, we are able to characterize the topological phase transition and study the effect of local operators (doping and magnetic fields) on the spatial localization of the parafermionic modes and their stability. Moreover, we discuss the necessary ingredients towards realizing \mathbb{Z}_3 parafermions in strongly interacting electronic systems.

I. INTRODUCTION

Quasiparticle excitations with non-Abelian exchange statistics have long been proposed as the as the building blocks of topological quantum computers [1]. Currently, the most promising candidate to this role are Majorana bound states (MBSs) [2, 3], with several proposals for their experimental realization being pursued [4, 5]. The basic mechanism is to use “braiding operations” of isolated MBS to encode and process information in “qubits” in a particular system. Such information is naturally protected by the non-Abelian nature of the braiding operations, which amounts to a “topological protection”.

A major limitation is that not all unitary operations (“quantum gates”) needed for a fully functional quantum computer can be emulated by MBS braiding. As such, some of the operations would not be topologically protected (and thus more susceptible to noise and decoherence effects), hindering the prospect of an all-Majorana-based universal quantum computer [1, 6, 7]. A possible solution to this problem is to use *parafermionic bound states*, which are natural generalizations of MBSs and could in principle be used as the building blocks of an universal topological quantum computer [8–10].

The concept of parafermions was introduced by Fradkin and Kadanoff in the context of clock-models in the early 80’s [11]. Parafermionic operators obey fractional statistics and also play an important role in critical behavior of clock-models and \mathbb{Z}_N -symmetric models [12]. Although parafermions were introduced in the context of statistical mechanics, they also arise as quasi-particle excitations in strong-correlated condensed matter [13–17].

In 1999, Read and Rezayi showed that the excitations of some Fractional Quantum Hall (FQH) states can be described using parafermions [18]. Parafermions in \mathbb{Z}_N models can have zero-energy edge states which are readily seen as a generalization of Majorana zero-modes [12, 19]. Although a topological computer made only by parafermions is not universal [20], \mathbb{Z}_3 parafermions can be used to produce “Fibonacci anyons” in 2D [8, 21],

leading to the interesting prospect of universal topological quantum computation using non-Abelian anyons [22].

Over the years, several models that host isolated parafermionic modes in condensed matter systems have been considered. Proposals range from interacting quantum wires [23, 24] to Abelian quantum Hall/superconductor hybrids and strongly interacting 2D topological insulator edges coupled to superconductors [22, 25]. Moreover, several recent works focus on the capability of a given system to host zero-mode parafermions through low-energy models [13, 17] and parafermion-only based Hamiltonians [26–28]. While the usual \mathbb{Z}_2 MBSs and, more recently, \mathbb{Z}_4 parafermionic zero modes [29] emerge as quasiparticle excitations in purely fermionic models (and thus can be detected by their “leakage” to side-coupled electronic quantum dots [30–32]), the picture for \mathbb{Z}_3 parafermionic modes is not quite clear. In fact, the question of whether purely fermionic models can produce (odd- N) \mathbb{Z}_N parafermionic edge modes is still an open one.

In this work, we address this fundamental question and propose a fermionic Hamiltonian that hosts \mathbb{Z}_3 parafermions. Our proposal is based on strong local electron-electron interactions such that fermionic double occupancy is suppressed. In a sense, the restriction to zero- and singly-occupied states plays a similar same role as the restriction to “spinless” fermions in the early proposals for Majorana bound states in semiconductor nanowires [2, 33–35].

In order to characterize the parafermionic phase, we use the density matrix renormalization group (DMRG) [36–38] to numerically calculate the energy gap, the entanglement entropy and the local spectral functions of the strongly correlated fermionic models. In addition, we study the stability of \mathbb{Z}_3 parafermions under effect of a local doping and the presence of a magnetic field, which can be an important for the prospects of parafermion-based topological quantum computation. We find that the parafermionic zero modes are stable against such local perturbations, as long as they preserve the \mathbb{Z}_3 symmetry.

The text is organized as follows. In Sec. II, we introduce a strongly-correlated fermionic model displaying \mathbb{Z}_3 parafermionic zero modes. By using a mean-field approach, we derive an effective model which maps exactly into a Kitaev-like \mathbb{Z}_3 parafermion chain. Moreover, in Sec. III we show that the derived Hamiltonians indeed display a \mathbb{Z}_3 phase and can be deformed into each other without closing the gap. The effect of local operators is studied in Sec. IV, where we show the existence of a topological phase transition between a topological phase with edge parafermionic modes and a non-topological normal state. We also discuss the dependence of edge modes and their robustness under effects of local operators. To this end, we introduce a Fock-parafermion spectral function that can be used to distinguish the edge states. Finally, we present our concluding remarks in Sec. V.

II. MODELS AND METHODS

In this section, we propose a spinful fermionic model supporting \mathbb{Z}_3 parafermionic edge modes. As previously discussed, the intrinsic difficulty in devising such a system is that the Hamiltonian must conserve parity symmetry (Z_2) and, at the same time, conserve a \mathbb{Z}_3 symmetry of the parafermionic modes, two mutually exclusive requirements. A possible solution is that the \mathbb{Z}_3 parafermionic modes emerge in a situation in which the parity of the different ground states is set by the number of sites in the chain. As we shall see, this is indeed the case in the proposed fermionic lattice models.

We begin by considering a fermionic spinful model with infinitely large on-site Hubbard repulsive interactions. In this limit, we can safely exclude the doubly-occupied state in the local Hilbert space of each site, a procedure akin to that used in the derivation of the t - J model [39]. The Hamiltonian reads

$$H_I = H^{(2)} + H^{(4)} + H^{(6)}, \quad (1)$$

where

$$H^{(2)} = \sum_{\substack{j=1 \\ \sigma=\uparrow,\downarrow}}^{L-1} -tc_{\sigma,j}^\dagger c_{\sigma,j+1} - \Delta c_{\sigma,j}^\dagger c_{-\sigma,j+1}^\dagger + H.c., \quad (2)$$

$$H^{(4)} = -W_4 \sum_{\substack{j=2 \\ \sigma=\uparrow,\downarrow}}^{L-1} c_{\sigma,j}^\dagger c_{-\sigma,j} c_{-\sigma,j+1}^\dagger c_{\sigma,j+1}, \quad (3)$$

$$H^{(6)} = -W_6 \sum_{\substack{j=2 \\ \sigma=\uparrow,\downarrow}}^{L-1} c_{\sigma,j-1}^\dagger c_{-\sigma,j-1} c_{\sigma,j}^\dagger c_{-\sigma,j} c_{\sigma,j+1}^\dagger c_{-\sigma,j+1}. \quad (4)$$

In the above, t is the single-particle hopping, Δ is a p-wave-like superconducting order parameter that mixes

spins in neighbour sites, W_4 is the strength of a synchronized spin-flip in two neighbour sites, while W_6 is the strength of synchronized spin-flip in three closest sites. We note that the three-body interaction contained in $H^{(6)}$ is an important ingredient for the existence of \mathbb{Z}_3 parafermions.

As a benchmark Hamiltonian supporting \mathbb{Z}_3 parafermionic edge modes, we can use a Kitaev-like parafermion chain with two dangling parafermions at the edges [12, 40], whose Hamiltonian is given by

$$H_{pf} = -J \sum_{j=1}^{L-1} \psi_j \chi_{j+1}^\dagger + H.c., \quad (5)$$

where each site has two parafermion modes ψ and χ satisfying parafermionic identities $\psi_j^\dagger = \psi_j^2$, $\chi_j^\dagger = \chi_j^2$ and $\chi_j \psi_j = \omega \psi_j \chi_j$, where $\omega = e^{2\pi i/3}$. For different sites, they satisfy a parafermionic exchange algebra $\psi_l \psi_j = \omega \psi_j \psi_l$, $\chi_l \chi_j = \omega \chi_j \chi_l$ and $\chi_l \psi_j = \omega \psi_j \chi_l$ for $l < j$.

This model is exactly solvable for any $J > 0$, showing a 3-fold degenerate ground state and a \mathbb{Z}_3 symmetry [12, 40, 41]. Moreover, one can show that H_{pf} can be written in terms of fermionic operators (see Appendix A) yielding a similar Hamiltonian as in the model proposed in Eq. (1).

We note that fermionization of H_{pf} produces a parity-violating interaction term $H^{(3)}$ given by

$$H^{(3)} = -W_3 \sum_{\substack{j=1 \\ \sigma=\uparrow,\downarrow}}^{L-1} (-1)^{\sum_{p<j} n_p} \left[c_{\sigma,j} c_{-\sigma,j+1}^\dagger c_{\sigma,j+1} + c_{\sigma,j}^\dagger c_{-\sigma,j} c_{\sigma,j+1}^\dagger \right] + H.c. . \quad (6)$$

This term corresponds to an exotic process of creation (annihilation) of an electron together with a spin-flip in the neighboring site. As such, it does not conserve parity nor the number of electrons. As discussed in Appendix B, this term should be understood as an effective mean-field interaction of the term $H^{(6)}$ given by Eq. (4) in which parity is spontaneously broken.

We thus define the following Hamiltonian H_{II} as

$$H_{II} = H^{(2)} + H^{(4)} + H^{(3)}. \quad (7)$$

For $J := t = \Delta = W_4 = W_3$, it can be shown (see Appendix B) that $H_{II} \rightarrow H_{pf}$. Moreover, as mentioned, one can establish an near equivalency between H_I (Eq. (1)) and H_{II} (Eq. (7)) in a mean-field limit, thereby establishing a regime of parameters in which H_I effectively hosts \mathbb{Z}_3 parafermionic modes. Such an equivalence of the fermionic model of Eq. (1) and the parafermionic chain of Eq. (5) is discussed in detail in Section III and constitutes one of the main results of the present work.

III. EQUIVALENCE OF THE MODELS

The existence of a \mathbb{Z}_3 phase in the Hamiltonian H_I can be established by two complementary methods. First, we

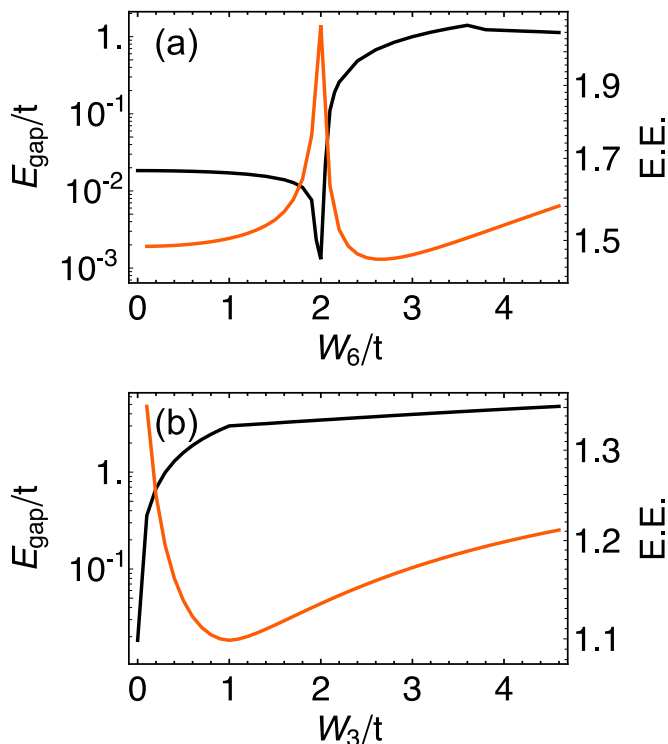


FIG. 1. Gap (black) and entanglement entropy (red) as a function of interaction strength (a) W_6 and (b) W_3 for the models described by H_I and H_{II} respectively. While the phase transition occurs at $W_6 > 2t$ in H_I , any $W_3 > 0$ induces the \mathbb{Z}_3 phase in H_{II}

show that there is a phase transition in which the ground state of the system goes from non-degenerate to three-fold degenerate. Then, we show that in this three-fold degenerate phase it is possible to smoothly deform H_I into H_{II} in a regime of parameters in which it displays the same \mathbb{Z}_3 parafermion phase as H_{pf} .

To this end, we obtain the overall ground states of the fermionic Hamiltonians as a function of the different Hamiltonian parameters with the DMRG method [36, 37, 42] as implemented within the ITensor package [38]. In the remainder of the paper, we use $t = \Delta = W_4$ and a 100-site chain, unless specified otherwise.

The topological phases can be characterized by two main quantities: the ground state degeneracy n_{gs} and the energy gap E_{gap} between the ground state and the first excited (many-body) state. We obtain n_{gs} in the DMRG calculations by counting the number of low-lying states within a window $\delta E \lesssim 10^{-3}t$ of the ground state energy (we take the hopping t as the energy unit). As discussed, this value is well within the ground-state energy accuracy in the DMRG calculations given the bond dimension and system's size. It is also enough to calculate E_{gap} : for the parameters used, $E_{gap} \gtrsim 10^{-2}t$ for all cases.

Results for E_{gap} for Hamiltonians H_I and H_{II} as a function of W_6 and W_3 respectively are shown in Fig. 1. Figure 1(a) shows E_{gap} for H_I as a function of W_6 . For

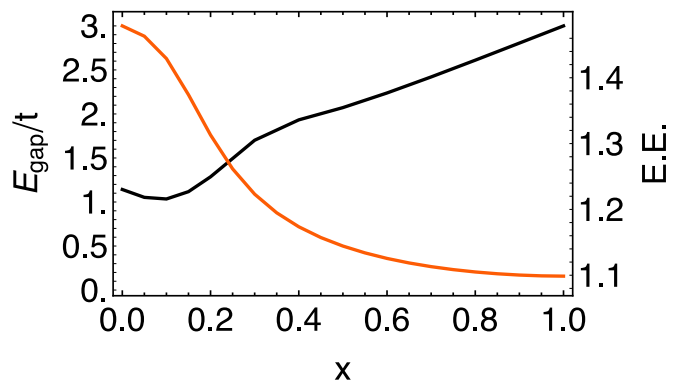


FIG. 2. Gap (black) and entanglement entropy (red) as a function of deformation parameter x , Eq. (8). We consider the case $W_6 = 3.2t$ and $W_3 = t$.

small values of W_6 , the system is in the trivial regime and has a small gap ($\sim 10^{-2}t$) which we attribute to finite-size effects. For $W_6 \approx 2t$, the system undergoes a phase transition, characterized by a sharp decrease in E_{gap} (“gap closing”) and an abrupt change in ground-state degeneracy from $n_{gs} = 1$ to $n_{gs} = 3$. The three-fold ground-state degeneracy characterizes the new phase as a \mathbb{Z}_3 (topological) phase.

Interestingly, the closing of the gap shown in Fig. 1(a) is accompanied by a discontinuity in the first derivative of the entanglement entropy (E. E.) [43]. At the \mathbb{Z}_3 phase, all ground states have a well defined \mathbb{Z}_2 parity which depends on the length L of the chain as $\hat{P}_{\mathbb{Z}_2} = (-1)^{\sum_i^L (n_{\uparrow,i} + n_{\downarrow,i})} = (-1)^{L \bmod 2}$. Moreover, these ground states are characterized by a \mathbb{Z}_3 symmetry operator $\hat{P}_{\mathbb{Z}_3} = \omega^{\sum_i^L (n_{\uparrow,i} + 2n_{\downarrow,i})}$. For this reason, the \mathbb{Z}_3 phase can not be understood as a combination of a Majorana-hosting phase together with a \mathbb{Z}_2 broken symmetry phase as it is the case for \mathbb{Z}_4 parafermions [27, 29, 32].

A similar analysis can be made for H_{II} , by plotting E_{gap} for increasing W_3 with $t = \Delta = W_4$ (Fig. 1(b)). The main difference is that the critical value in which the system goes from the trivial to \mathbb{Z}_3 phase is $W_3 = 0$. As such, for any $W_3 > 0$ the system is in the \mathbb{Z}_3 phase and no phase transition takes place for non-zero values of W_3 , as indicated by the absence of a peak in the entanglement entropy. In fact, the E.E. reaches its minimum value ($\log(3)$) for $W_3 = t$, precisely the point where the mapping of H_{II} to the parafermion chain Hamiltonian H_{pf} is exact. Moreover, the existence of \mathbb{Z}_3 parafermionic zero modes in the double-occupancy regime is discussed in Appendix C.

In order to confirm that the limits of large W_6 in H_I and large W_3 for H_{II} correspond to the same topological \mathbb{Z}_3 phase, we consider the following Hamiltonian:

$$H'(x) = (1-x)H_I + xH_{II}, \quad (8)$$

which is equal to H_I and H_{II} for $x=0$ and $x=1$ respectively. In a sense, x acts as a parameter which continu-

ously “deforms” $H^{(6)}$ into $H^{(3)}$.

Figure 2 shows the dependency of E_{gap} and entanglement entropy with x for $W_6 = 3.2t$ and $W_3 = t$. The crucial result is that there is no gap closing or sharp features in the entanglement entropy (which would be indicative of a phase transition) as x varies from 0 to 1. In fact, the minimum gap is $E_{\text{gap}} \approx t$ for $x = 0.1$ and the difference in the entanglement entropy’s value is due the differences in the ground states occupancies. This shows that both Hamiltonians describe the same \mathbb{Z}_3 topological phase for these values of W_6 and W_3 .

IV. EFFECTS OF LOCAL OPERATORS

Although both H_I and H_{II} display a parafermion-hosting \mathbb{Z}_3 phases, the ground states themselves are very different. For example, the H_I ground state has a well defined parity, while H_{II} ground state does not. Nonetheless, we expect the general behavior of parafermions under changes in local operators to be similar. Since the DMRG calculations are a few orders of magnitude faster for H_{II} , we will use it as a “benchmark” in this Section. In the following, we set $W_3 = t$ (and $W_6 = 0$) meaning that, in the absence of other terms in the Hamiltonian, the system will be in the topological phase of H_{II} .

Previous studies [12, 40] have shown that local interactions might be able to destroy the parafermion phase. Specifically, the interaction $-f(e^{i\theta}\psi_j^\dagger\chi_j + e^{-i\theta}\chi_j^\dagger\psi_j)$ destroys the parafermion edge while conserving the FPF number. In particular, there is a phase transition at $f=J$ with $\theta=0$. This interaction translates into the fermionic language (see Appendix A) as

$$e^{i\theta}\psi_i^\dagger\chi_i + e^{-i\theta}\chi_i^\dagger\psi_i = -2\sqrt{3}\sin(\theta)n_{\uparrow,i} + [3\cos(\theta) - \sqrt{3}\sin(\theta)]n_{\downarrow,i}, \quad (9)$$

which can be thought as a mixing of magnetic field and chemical potential for any θ . This shows the importance of local operators to parafermions. In particular, we are interested in the effects of chemical potential

$$H_d = - \sum_{\substack{j=1 \\ \sigma=\uparrow,\downarrow}}^L \mu n_{\sigma,j}, \quad (10)$$

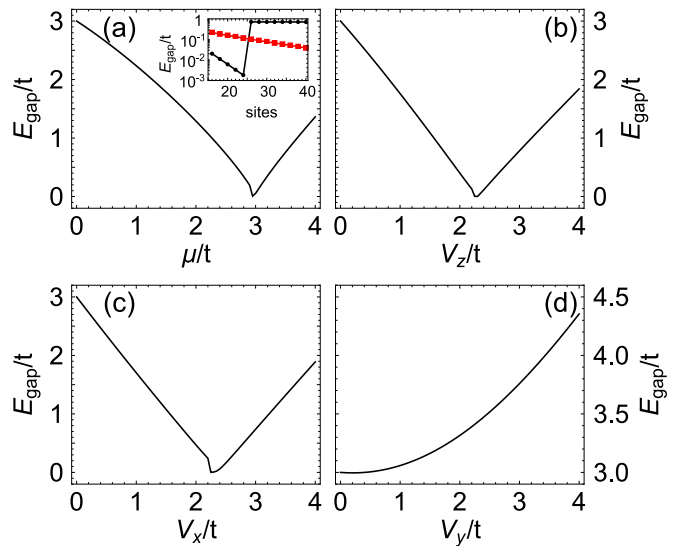


FIG. 3. Dependence of the gap (Δ) with respect to local operators. (a) Doping (μ), (b) z-direction (V_z), (c) x-direction (V_x), and (d) y-direction (V_y) Zeeman terms. Panels (a) and (b) show a topological phase transition at $\mu = 3t$ and $V_z = 2.3t$ respectively. Panel (c) has a phase transition between a twofold degenerate state to a normal state for $V_x \approx 2.5J$. Finite-size effects are responsible for the discontinuity in the gap. Figure (d) shows no phase transition as a function of V_y , and the gap always increases. The inset in panel (a) shows the exponential dependence of the gap between the parafermionic modes with the chain length for $\mu = 2.5t$ (black circles) and $\mu = 2.9t$ (red squares).

and Zeeman fields in all three directions:

$$H_x = \sum_{\substack{j=1 \\ \sigma=\uparrow,\downarrow}}^L V_x c_{\sigma,j}^\dagger c_{-\sigma,j}, \quad (11)$$

$$H_y = \sum_{\substack{j=1 \\ \sigma=\uparrow,\downarrow}}^L -iV_y \sigma c_{\sigma,j}^\dagger c_{-\sigma,j}, \quad (12)$$

$$H_z = \sum_{\substack{j=1 \\ \sigma=\uparrow,\downarrow}}^L V_z \sigma n_{\sigma,j}, \quad (13)$$

which will be added to H_{II} .

A. Energy gap

Figure 3 shows the dependence of the gap energy E_{gap} with each of these local terms for a 100-site chain. Regarding the chemical potential (μ), we see a near gap closing at $\mu \approx 2.9t$ (Fig. 3(a)). This is consistent with previous results [40] which show a transition between

topological (parafermionic) and normal phases for $\mu=3t$. We believe the small discrepancy with our result can be accounted for by finite-size effects. In fact, we can verify that the phase transition point approaches $\mu=3t$ for increasing the chain sizes (see Section IV B).

The inset of Fig. 3(a) shows that the gap between the parafermion states decrease exponentially in the topological phase. This gap arises due the coupling between parafermionic modes located at the both ends of the chain. This exponential decay depends on μ [44], as illustrated by the slower decay with size by $\mu=2.9t$ as compared to the case $\mu=2.5t$. As such, this is equivalent to the ‘‘exponential protection’’ predicted for Majorana modes [45] and was also predict to occur for \mathbb{Z}_4 parafermions as well [29].

Parafermionic edge modes are also stable under a small local Zeeman-like term in the z-direction proportional to V_z , as given by Eq. (13). As shown in Fig. 3(b), the topological phase is destroyed only for relatively large values of the Zeeman term ($V_z \gtrsim 2.3t$). In addition, similarly to the dependency with the doping μ , the transition value is sensitive to finite size-effects even for long chains. In both cases (μ and V_z), the ground state goes from a 3-fold degenerate to a non-degenerate one at the transition.

As discussed in detail in Appendix A, a generic magnetic field in the xy plane does *not* conserve the Fock-parafermion number, thus breaking the \mathbb{Z}_3 symmetry. In fact, any small positive Zeeman term in the x -direction ($V_x > 0$) breaks the ground state \mathbb{Z}_3 symmetry, changing the ground state degeneracy from $n_{gs}=3$ to $n_{gs}=2$. As V_x increases, a second phase transition occurs, further reducing n_{gs} from 2 to 1. This is shown in Fig. 3(c), where the phase transition to the $n_{gs}=1$ (non-degenerate) ground state occurring around $V_x \approx 2.5t$. In this case, finite-size effects are more prominent than the previous cases, making it difficult to pinpoint the exact V_x value where phase transition occurs for large systems.

By contrast, any positive Zeeman term in the y direction ($V_y > 0$) produces a phase transition directly from $n_{gs}=3$ to $n_{gs}=1$. The gap increases monotonically with V_y , as shown in Fig. 3(d). Due to these differences between x and y -directions, we expect a strong dependence of the gap with the direction of magnetic fields in the xy -plane.

In order to better understand how the local Zeeman terms in the xy -plane affect the parafermionic chain ground state, we consider a generic Zeeman term arising from a magnetic field in the xy -plane, given by

$$H_{xy} = V_{xy} \sum_{j=1}^L e^{-i\theta} c_{\uparrow,j}^\dagger c_{\downarrow,j} + e^{i\theta} c_{\downarrow,j}^\dagger c_{\uparrow,j}, \quad (14)$$

where $V_{xy} = \sqrt{V_x^2 + V_y^2}$ is the strength of Zeeman field and θ is the magnetic field angle in respect to x -direction.

We calculate the gap energy (E_{gap}) and ground state degeneracy (n_{gs}) as a function of V_{xy} and θ . The results are depicted in Fig 4. Notice the clear symmetry in $E_{\text{gap}}(\theta)$ and $n_{gs}(\theta)$ as $\theta \rightarrow \theta + 2\pi/3$. This is in

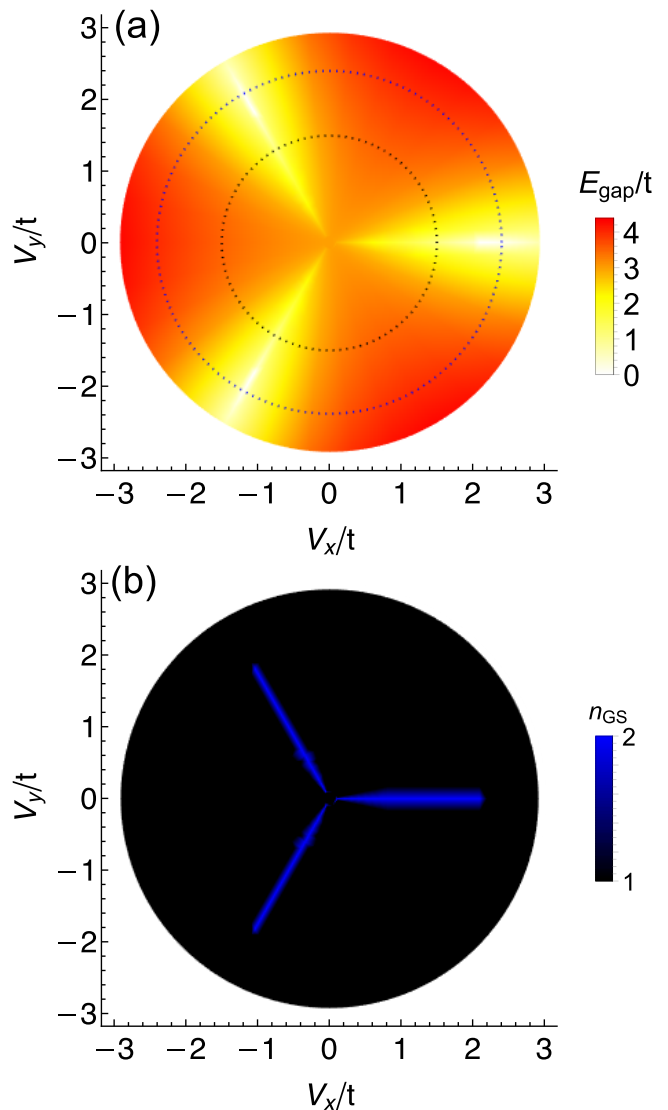


FIG. 4. Dependence of (a) gap to the intensity and angle of magnetic field, upper figure, and (b) its ground state degeneracy, n_{gs} , lower figure. For fixed $V_{xy} < 2.5t$ the gap is minimum at angles $0, \pm 2\pi/3$ and the ground state is twofold degenerate. The dotted circles in (a) corresponds to the transversal cut shown in Fig. 5.

fact due to the invariance of H_{xy} under a $2\pi/3$ -rotation, associated with the \mathbb{Z}_3 symmetry of the full Hamiltonian. This invariance becomes clear by writing Eq. (14) in terms of parafermion operators, which can be accomplished by inverting the fermionization process discussed in Appendix A. The result is:

$$H_{xy} = \frac{V_{xy}}{3} \sum_{j=1}^L \omega^{\sum_{p<j} N_p} e^{-i\theta} \left[\chi_j + \omega \psi_j + \chi_j^\dagger \psi_j^\dagger \right] + \omega^2 \sum_{p<j} N_p e^{i\theta} \left[\chi_j^\dagger + \omega^2 \psi_j^\dagger + \omega^2 \chi_j \psi_j \right]. \quad (15)$$

For $\theta = 0$ and $\pm 2\pi/3$, the Hamiltonian is invariant

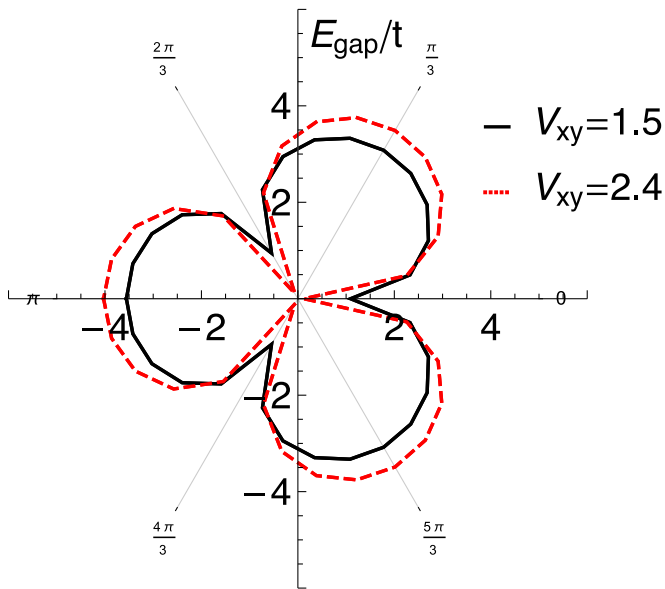


FIG. 5. Transversal cut of Fig. 4 with $V_{xy} = 1.5t$, solid black, and $V_{xy} = 2.4t$, dashed red.

under a transformation $\chi \rightarrow e^{i\theta}\chi$ and $\psi \rightarrow e^{i\theta}\psi$. This can be easily seen in Fig. 4, where the smallest gaps occur at angles $\theta_n^{\min} = 2n\pi/3$, $n = 1, 2, 3$. In those cases, the ground state is doubly-degenerate, as discussed above, with a phase transition occurring at $V_{xy} \approx 2.5t$, similar that shown in Fig. 3(c).

In order to better visualize this, a crosscut of Fig. 4 with $V_{xy} = 1.5t$ and $V_{xy} = 2.4t$ is shown in Fig. 5. The minimum gap occurs $\theta_n^{\min} = 2n\pi/3$ and the maxima are at $\theta_n^{\max} = (2n-1)\pi/3$ with $n = 1, 2, 3$.

B. Fock-parafermion spectral function

We now turn to the spatial distribution of the parafermionic modes along the chain. To this end, we calculate the zero-energy Fock parafermion spectral function at site j defined as:

$$\mathcal{A}_j(0) = \frac{2\pi}{n_{\text{gs}}} \sum_{k=1}^2 \sum_{|\varphi\rangle, |\varphi'\rangle} |\langle \varphi' | d_j^k | \varphi \rangle|^2 + |\langle \varphi' | d_j^{\dagger k} | \varphi \rangle|^2, \quad (16)$$

where d is the Fock-parafermion operator defined in Eq. (A4) in Appendix A and the second summation (normalized by the ground states degeneracy n_{gs}) runs over all ground states $\{|\varphi\rangle\}$ [46].

For a parafermion chain with no local interactions (Eq. (5)), the zero-energy FPF spectral function is $\mathcal{A}_j(0)/(2\pi) = 4/9(\delta_{j,1} + \delta_{j,L})$, which is perfectly consistent with our simulations. In the supplementary materials, Sec. D, we show the derivation for the analytic values of $\mathcal{A}_j(0)$ a generic \mathbb{Z}_M parafermion.

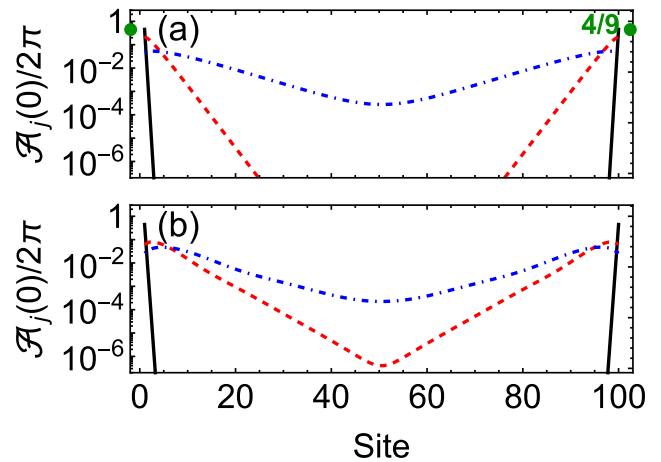


FIG. 6. FPF spectral function $\mathcal{A}_j(0)$ for different interactions. (a) Spread of ground-state over the chain for different chemical potentials $\mu = 0.1t$ (solid black), $\mu = 2.5t$ (dashed red) and $\mu = 2.8t$ (dot-dashed blue). The green dots mark the analytical value $(4/9)$ for a perfectly localized \mathbb{Z}_3 edge parafermions. (b) Spread of ground-state over the chain for z-direction Zeeman $V_z = 0.1t$ (solid black), $V_z = 2.1t$ (dashed red) and $V_z = 2.2t$ (dot-dashed blue)

We emphasize that $\mathcal{A}_j(0)$ measures the local density of states related to Fock-parafermions instead of the electrons, although the actual calculations involve fermionic matrix elements. A more naïve approach would be to calculate the purely fermionic spectral function, as it has been done in the \mathbb{Z}_4 case [29, 32]. However, the fermionic spectral function does not capture the localized edge parafermionic states since the ground states $\{|\varphi\rangle\}$ of H_{II} do not have a well defined parity. In addition, the terms arising from bulk states do not necessarily cancel each other as it happens for $\mathcal{A}_j(0)$ (see Appendix D). Overall, $\mathcal{A}_j(0)$ is a better option to visualize the overlap between parafermionic modes.

Figure 6(a) shows the spreading of the parafermionic state along the 100-site chain as we increase the doping across the phase transition at $\mu \approx 2.9$. The plot of $\mathcal{A}_j(0)$ shows exponentially localized modes in the topological phase ($\mu = 0.5t$ (black) and $\mu = 2.5t$ (dashed red)), while the ground state becomes delocalized near the transition point ($\mu = 2.8t$ (dashed blue)). Moreover, it becomes clear that finite-size effects can be considerable in small chains (< 100 sites long).

The same analysis can be done the case of a magnetic field in the z-direction (Fig. 6(b)) for $\mu = 0.1t$. Again, the spectral function show exponentially localized edge modes for $V_z < V_z^c = 2.2t$, i.e., before the phase transition at $V_z^c = 2.2t$ (dashed blue curve), at which point the ground-state spectral function is spread all over the chain.

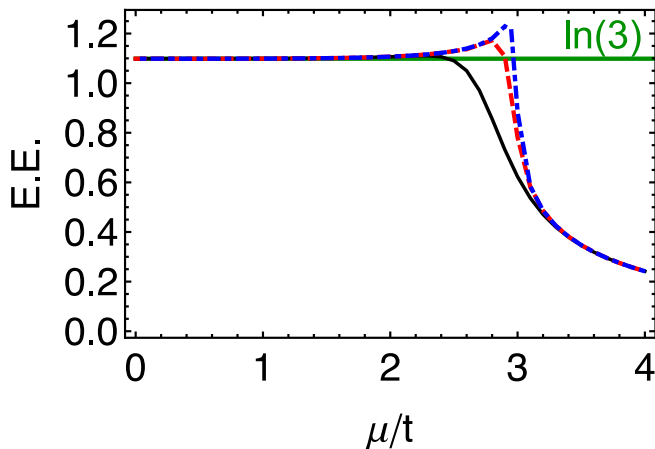


FIG. 7. Entanglement entropy (E.E.) dependence with doping for different chain length, 16 (solid black), 48 (dashed red), 100 (dotted blue). Note that far away from the phase transition all of them have the same value.

C. Entanglement entropy

Last, we consider the signatures of the topological phase transition in the entanglement entropy (E.E.) [40, 47]. Figure 7 shows the E.E. calculated at the central link of the chain as a function of the chemical potential μ for different chain sizes.

For small values of μ such that the system is in the topological phase, E.E. is constant and pinned at $\ln(3)$ (main panel of Fig. 7). This is consistent with previous DMRG results for \mathbb{Z}_3 parafermion chains [40]. As μ increases and the system approaches the topological phase transition, the E.E. increases, reaches a maximum near the phase transition and then decreases. This behavior is accentuated for larger chains, as shown in Fig. 7.

V. CONCLUDING REMARKS

In conclusion, in this paper we study a family of purely 1D fermionic models which map into a Kitaev-like chain of \mathbb{Z}_3 parafermions. Similarly to the case of Majorana zero modes, the system has a topological phase with exponentially localized \mathbb{Z}_3 parafermionic modes at its ends.

A key element in the proposed models is the presence of strong, Hubbard-like, repulsive interaction of strength U_H on each site of the fermionic chain, effectively restricting the local Hilbert space to a $t-J$ model-like basis of zero- and singly occupied (spinful) fermionic states. Within this basis, an exact mapping of the parafermion chain to a fermionic model is obtained. Even though the mapping is exact only in the $U_H \rightarrow \infty$ limit, we show (see Appendix C) that the parafermionic phase is present even for moderate values of the interaction in the range $U_H/t \gtrsim 10$.

Although this mapping produces non-physical parity-breaking terms, we show that such terms can be understood as a mean-field reduction of a parity-preserving 3-body interaction term. In fact, we establish that this rather exotic 3-body, spin-flipping interaction term is directly responsible for the existence of a \mathbb{Z}_3 symmetry-protected topological phase with parafermionic edge modes. More importantly, we show that the ground state of the resulting Hamiltonian does have a well-defined parity and cannot be understood as a combination of symmetry-broken \mathbb{Z}_2 Majorana modes.

Our DMRG calculations show topological phase transitions as a function of several parameters. We show that phase transitions can be characterized by different metrics such as many-body gap closings and openings, changes in the ground state degeneracy and peaks in the entanglement entropy.

These calculations confirm the topological equivalency of the fermionic models and the parafermion chain and provide a way to probe the robustness of the topological phase against one-body terms such as onsite Zeeman field in z -direction and changes in the chemical potential. In particular, we show that an in-plane (xy) magnetic field can produce phase transitions depending on the angle θ between x and y components. This produces an 3-fold anisotropy in the energy gap and ground state degeneracy with θ stemming from the expected \mathbb{Z}_3 symmetry of the original fermionic Hamiltonian.

Moreover, the Fock-parafermion spectral function (FPF-SF) confirms the exponential localization of the parafermionic modes deep in the topological regime and for large. As the system approaches the phase transition, the FPF-SF becomes more delocalized as the edge modes located at opposite ends of the chain overlap with each other. Such finite-size effects turn out to be very relevant for small chains (less than ~ 100 sites).

Finally, while these results are an important step in understanding how \mathbb{Z}_3 (and, more generally odd- N \mathbb{Z}_N) parafermionic modes can emerge in purely fermionic systems, there are certainly several questions open. For instance: Can one detect \mathbb{Z}_3 parafermionic modes using coupling to real fermions as in the \mathbb{Z}_4 case [32]? Can these modes be used to produce topologically-protected Fibonacci anyons [8]? Do these modes have different braiding statistics from pure (non-fermionic) \mathbb{Z}_3 parafermions, similar to \mathbb{Z}_4 parafermions [27]? These are all relevant questions which should be explored in future works on the topic.

ACKNOWLEDGMENTS

We thank Thomas Schmidt for enlightening discussions. We acknowledge financial support from Brazilian agencies FAPESP (Grant no. 2019/11550-8), Capes, and CNPq (Graduate scholarship program 141556/2018-8, and Research Grants 308351/2017-7, 423137/2018-2, and 309789/2020-6).

Appendix A: Fermionization

In order to find a representation of the Hamiltonian H_{pf} (given by Eq. (5)) and its parafermions in terms of fermionic operators, it is useful to consider Fock-parafermions (FPF) operators [29, 48]. These operators act in the space of states with a well-defined Fock-parafermion number. Each parafermion can be described in terms of creation (d^\dagger) or annihilation (d) operators, which, respectively, increase or decrease the FPF number, as:

$$\psi_j = d_j \omega^{N_j} + d_j^{\dagger 2} \quad \chi_j = d_j + d_j^{\dagger 2}, \quad (\text{A1})$$

where $N_j = d_j d_j^\dagger + d_j^2 d_j^{\dagger 2}$ is the number of FPF and can be either 0, 1 or 2. Because of Eq. (A1), FPF operators must satisfy relations similar to parafermions [48],

$$\begin{aligned} d_j d_l &= \omega d_l d_j, & d_j d_l^\dagger &= \omega d_l^\dagger d_j, & \text{for } l < j \\ d^3 &= d^{\dagger 3} = 0 \\ d_j^{\dagger m} d_j^m + d_j^{3-m} d_j^{\dagger 3-m} &= 1 & \text{for } m = 1, 2 \end{aligned} \quad (\text{A2})$$

In order to represent operator d in a fermionic representation, we choose a mapping between FPF number and fermionic number basis such that each state in the t - J fermionic basis [39] ($|E\rangle, c_\uparrow^\dagger|E\rangle, c_\downarrow^\dagger|E\rangle$, with $|E\rangle$ a vacuum state) corresponds to one state in the FPF number basis ($|0\rangle, |1\rangle, |2\rangle$). This mapping can be summarized as

$$\begin{aligned} |2\rangle &\xrightarrow{d} |1\rangle \xrightarrow{d} |0\rangle \xrightarrow{d} \emptyset \\ c_\downarrow^\dagger|E\rangle &\xrightarrow{d} c_\uparrow^\dagger|E\rangle \xrightarrow{d} |E\rangle \xrightarrow{d} \emptyset. \end{aligned} \quad (\text{A3})$$

With this in mind, it is straightforward to find a representation of FPF operators, $d = c_\uparrow + c_\uparrow^\dagger c_\downarrow$. It is also easy to see that Eq (A3) satisfies all FPF operator relations. However, since the FPF operators operate in real space (sites in a chain), we need to consider Jordan-Wigner string factors for both FPF operators and fermionic operators [29, 48]

$$d_j = \omega^{\sum_{p<j} N_p} \left[(-1)^{\sum_{p<j} n_p} c_{\uparrow,j} + c_{\uparrow,j}^\dagger c_{\downarrow,j} \right], \quad (\text{A4})$$

$$d_j^2 = \omega^{\sum_{p<j} 2N_p} \left[(-1)^{\sum_{p<j} n_p} c_{\downarrow,j} \right], \quad (\text{A5})$$

where n_p is the occupation number (0 or 1) of site p and $N_p = n_{\uparrow,p} + 2n_{\downarrow,p}$.

An important consequence of these strings is that FPF operators have two distinct long-range behaviors, namely (i) a JW-like string which depends on the FPF number N_p applied uniformly to terms and (ii) a JW string which depends on the fermionic occupation n_p applied only on single fermion operators. This is distinct than in the case of \mathbb{Z}_4 parafermions where all terms have the same parity

and string factor [49]. This means that, apart from the expected Jordan-Wigner string, the Hamiltonian is local in the FPF space (although non-local in the fermionic basis), allowing one to derive local quantities that identify the edge states.

The dangling parafermions at the chain edges can be easily written in terms of fermions, as

$$\chi_1 = c_{\uparrow,1} + c_{\downarrow,1}^\dagger + c_{\uparrow,1}^\dagger c_{\downarrow,1}, \quad (\text{A6})$$

$$\psi_L = \omega^{\sum_{p<L} N_p} \left[(-1)^{\sum_{p<L} n_p} [\omega c_{\uparrow,L} + c_{\downarrow,L}^\dagger] + \omega^2 c_{\uparrow,L}^\dagger c_{\downarrow,L} \right].$$

Notice that ψ_L contains information of the fermionic occupation in the central chain sites. This means that the edge modes are affected by the bulk states via Jordan-Wigner strings. While this also occurs in the \mathbb{Z}_4 case [29], the difference here is that the strings are not applied uniformly in every term, due to absence of a well-defined parity of the operators.

Appendix B: Mean-field derivation

In this appendix, we use mean-field arguments to obtain an expression similar to Eq. (6) starting from Eq. (4).

We start with the spin-up terms in Eq. (4):

$$\begin{aligned} c_{\uparrow,i-1}^\dagger c_{\downarrow,i-1} c_{\uparrow,i}^\dagger c_{\downarrow,i} c_{\uparrow,i+1}^\dagger c_{\downarrow,i+1} &\approx \\ \langle c_{\uparrow,i-1}^\dagger c_{\downarrow,i-1} c_{\uparrow,i}^\dagger \rangle c_{\downarrow,i} c_{\uparrow,i+1}^\dagger c_{\downarrow,i+1} &+ \\ \langle c_{\uparrow,i-1}^\dagger c_{\downarrow,i-1} c_{\downarrow,i} \rangle c_{\uparrow,i}^\dagger c_{\uparrow,i+1}^\dagger c_{\downarrow,i+1} &+ \\ c_{\uparrow,i-1}^\dagger c_{\downarrow,i-1} c_{\uparrow,i}^\dagger \langle c_{\downarrow,i} c_{\uparrow,i+1}^\dagger c_{\downarrow,i+1} \rangle &+ \\ c_{\uparrow,i-1}^\dagger c_{\downarrow,i-1} c_{\downarrow,i} \langle c_{\uparrow,i}^\dagger c_{\uparrow,i+1}^\dagger c_{\downarrow,i+1} \rangle & \end{aligned} \quad (\text{B1})$$

where we use the commutation relation $[c_{\uparrow,i}^\dagger, c_{\downarrow,j}] = \delta_{i,j} c_{\uparrow,i}^\dagger c_{\downarrow,i}$ arising from the t - J model requirement of exclusion double occupancy states.

Assuming a spatially isotropic and spin $SU(2)$ -symmetric, the expectation values in Eq. (B1) should be proportional to $(-1)^{\sum_{p<i} n_p}$. As such, we recover the mean-field interaction:

$$\begin{aligned} H_{MF}^{(6)} &= -W_{MF} \sum_j^{L-1} (-1)^{\sum_{p<j} n_p} \left[(c_{\uparrow,j} + c_{\downarrow,j}^\dagger) c_{\downarrow,j+1}^\dagger c_{\uparrow,j+1} + \right. \\ &\quad \left. + c_{\uparrow,j}^\dagger c_{\downarrow,j} (c_{\uparrow,j+1}^\dagger + c_{\downarrow,j+1}) \right] + H.c. \end{aligned} \quad (\text{B2})$$

which is the same as Equation (6) for an infinite chain, i.e. without edges.

Notice, however, this method does not generate interaction at the edge sites. This is, in part, the reason why we need long chains ($\gtrsim 100$ sites) to describe \mathbb{Z}_3 edge parafermions using the model described by H_I (as discussed in Sec. III), while, at the same time, these modes already appear for small chains (~ 16 sites) when the effective model H_{II} is used in the calculations.

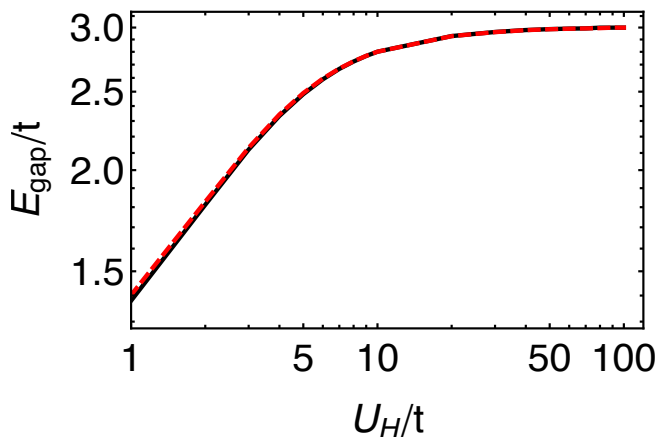


FIG. 8. Gap dependency with Hubbard interaction in a double occupancy basis. The gap of 16-sites chain (red dashed) and 100-site chain (solid black) have minor differences only in the low interaction regime, $U_H \approx t$.

Appendix C: Double occupancy basis

In the previous sections, we considered a local fermionic basis excluding the double occupancy state, $c_{\downarrow}^{\dagger} c_{\uparrow}^{\dagger} |E\rangle$. A consistency check for this approach would be to include this state in the fermionic basis along with a Hubbard interaction in each site, $U_H n_{\uparrow} n_{\downarrow}$ and then take the limit $U_H \rightarrow \infty$. In this Appendix, we perform this consistency check and show that indeed we recover the main text's results.

Figure 8 illustrates the persistence of the parafermionic phase already for relatively small values of U_H relative to the hopping t (say, $U_H/t \sim 1 - 5$. For $U_H \gg t$, the gap becomes completely independent of the chain size, and we recover the expected $E_{\text{gap}}/t=3$. This shows that a large Hubbard (on-site) interaction is not necessary for the formation of \mathbb{Z}_3 parafermions and that finite-size effect are not relevant in this regime.

Appendix D: FPF spectral function derivation

In this section, we show that the FPF spectral function for a \mathbb{Z}_M parafermion chain with two dangling parafermions described by Eq. (5) is given by $\mathcal{A}_j = 2\pi \frac{2(M-1)}{M^2} (\delta_{1,j} + \delta_{L,j})$.

We start with the FPF spectral function, defined by Eq. (16). We can write it as:

$$\mathcal{A}_j(E') = 2\pi \sum_{k=1}^{N-1} \sum_{|\varphi\rangle} \delta(E' + E_{\varphi} - E_0) |\langle \varphi | d_j^k | g_0 \rangle|^2 + \delta(E' - E_{\varphi} + E_0) |\langle \varphi | d_j^{\dagger k} | g_0 \rangle|^2, \quad (\text{D1})$$

where $|g_0\rangle$ is one ground state and $|\varphi\rangle$ is an eigenstate of the Hamiltonian. We consider the M ground states $|f_i\rangle$, with f_i being the FPF number, such that $\langle f_j | d^k | f_i \rangle = \delta_{j,i-k}$ and $\langle f_j | d^{\dagger k} | f_i \rangle = \delta_{j,i+k}$.

For a generic chain with L sites, the ground state with FPF number i [41] is given by

$$|g_i^L\rangle = \frac{1}{\sqrt{M^{L-1}}} \sum_{\substack{\{N_j\} \text{ such that} \\ \sum_j N_j = i \pmod M}} \bigotimes_{j=1}^L |N_j\rangle, \quad (\text{D2})$$

which, in turn, can be written in terms of a chain with $L-1$ sites and a single site at one of the ends or a single site at position s and two chains with $s-1$ and $L-s$ sites.

$$|g_i\rangle = \frac{1}{\sqrt{M}} \sum_{k=0}^{M-1} |f_{i-k}\rangle \otimes |g_k^{L-1}\rangle \quad (\text{D3})$$

$$|g_i\rangle = \frac{1}{\sqrt{M}} \sum_{k=0}^{M-1} |g_k^{L-1}\rangle \otimes |f_{i-k}\rangle \quad (\text{D4})$$

$$|g_i\rangle = \frac{1}{M} \sum_{a=0}^M \sum_{k=0}^{M-1} |g_a^{s-1}\rangle \otimes |f_{i-k}\rangle \otimes |g_{-a+k}^{L-s}\rangle, \quad (\text{D5})$$

It is straightforward to see that at positions 1 and L we have $|\langle g_{i-k} | d^k | g_i \rangle|^2 = 1/M^2$. In the bulk, Eq. (D5), we need to consider the FPF commutation relations, Eq. (A2).

Applying d_s at $|g_i\rangle$, with s in the bulk, does not only decrease the FPF number in one but also add a phase that depends on the FPF number that precedes it,

$$d_s |g_i\rangle = \frac{1}{M} \sum_{a=0}^M \sum_{k=0}^{M-1} e^{2\pi i a/M} |g_a^{s-1}\rangle \otimes |f_{i-k-1}\rangle \otimes |g_{-a+k}^{L-s}\rangle, \quad (\text{D6})$$

such that $\langle g_j | d_s | g_i \rangle \propto \delta_{j,i-1} \sum_{a=0}^{M-1} e^{2\pi i a/M} = 0$. Therefore, for a spectral function, at zero energy, that takes into account all d^k , for k between 1 and $M-1$,

$$\mathcal{A}_j = 2\pi \sum_{p=1}^{M-1} \sum_{|g\rangle} |\langle g | d_j^p | g_0 \rangle|^2 + |\langle g | d_j^{\dagger p} | g_0 \rangle|^2, \quad (\text{D7})$$

where the sum in $|g\rangle$ is over all ground states, and

- [1] C. Nayak, S. H. Simon, A. Stern, M. Freedman, and S. Das Sarma, Non-abelian anyons and topological quantum computation, *Rev. Mod. Phys.* **80**, 1083 (2008).
- [2] A. Y. Kitaev, Unpaired majorana fermions in quantum wires, *Physics-Uspekhi* **44**, 131 (2001).
- [3] D. Aasen, M. Hell, R. V. Mishmash, A. Higginbotham, J. Danon, M. Leijnse, T. S. Jespersen, J. A. Folk, C. M. Marcus, K. Flensberg, and J. Alicea, Milestones toward majorana-based quantum computing, *Phys. Rev. X* **6**, 031016 (2016).
- [4] R. M. Lutchyn, E. P. A. M. Bakkers, L. P. Kouwenhoven, P. Krogstrup, C. M. Marcus, and Y. Oreg, Majorana zero modes in superconductor–semiconductor heterostructures, *Nature Reviews Materials* **3**, 52 (2018).
- [5] K. Flensberg, F. von Oppen, and A. Stern, Engineered platforms for topological superconductivity and majorana zero modes, *Nature Reviews Materials* **6**, 944 (2021).
- [6] A. Stern and N. H. Lindner, Topological quantum computation—from basic concepts to first experiments, *Science* **339**, 1179 (2013), <http://science.sciencemag.org/content/339/6124/1179.full.pdf>.
- [7] S. D. Sarma, M. Freedman, and C. Nayak, Majorana zero modes and topological quantum computation, *Npj Quantum Information* **1**, 15001 EP (2015), review Article.
- [8] E. M. Stoudenmire, D. J. Clarke, R. S. K. Mong, and J. Alicea, Assembling fibonacci anyons from a F_3 parafermion lattice model, *Phys. Rev. B* **91**, 235112 (2015).
- [9] A. Hutter and D. Loss, Quantum computing with parafermions, *Phys. Rev. B* **93**, 125105 (2016).
- [10] E. Cobanera, J. Ulrich, and F. Hassler, Changing anyonic ground degeneracy with engineered gauge fields, *Phys. Rev. B* **94**, 125434 (2016).
- [11] E. Fradkin and L. Kadanoff, Disorder variables and parafermions in two-dimensional statistical mechanics, *Nuclear Physics B* **170**, 1 (1980).
- [12] P. Fendley, Parafermionic edge zero modes in z_n -invariant spin chains, *Journal of Statistical Mechanics: Theory and Experiment* **2012**, P11020 (2012).
- [13] C. Fleckenstein, N. T. Ziani, and B. Trauzettel, F_4 parafermions in weakly interacting superconducting constrictions at the helical edge of quantum spin hall insulators, *Phys. Rev. Lett.* **122**, 066801 (2019).
- [14] Y. Alavirad, D. Clarke, A. Nag, and J. D. Sau, F_3 parafermionic zero modes without andreev backscattering from the $2/3$ fractional quantum hall state, *Phys. Rev. Lett.* **119**, 217701 (2017).
- [15] A. Vaezi, Superconducting analogue of the parafermion fractional quantum hall states, *Phys. Rev. X* **4**, 031009 (2014).
- [16] Y. Vinkler-Aviv, P. W. Brouwer, and F. von Oppen, F_4 parafermions in an interacting quantum spin hall josephson junction coupled to an impurity spin, *Phys. Rev. B* **96**, 195421 (2017).
- [17] J. Klinovaja and D. Loss, Parafermions in an interacting nanowire bundle, *Phys. Rev. Lett.* **112**, 246403 (2014).
- [18] N. Read and E. Rezayi, Beyond paired quantum hall states: Parafermions and incompressible states in the first excited landau level, *Phys. Rev. B* **59**, 8084 (1999).
- [19] A. S. Jermyn, R. S. K. Mong, J. Alicea, and P. Fendley, Stability of zero modes in parafermion chains, *Phys. Rev. B* **90**, 165106 (2014).
- [20] R. S. K. Mong, D. J. Clarke, J. Alicea, N. H. Lindner, P. Fendley, C. Nayak, Y. Oreg, A. Stern, E. Berg, K. Shtengel, and M. P. A. Fisher, Universal topological quantum computation from a superconductor-abelian quantum hall heterostructure, *Phys. Rev. X* **4**, 011036 (2014).
- [21] D. J. Clarke, J. Alicea, and K. Shtengel, Exotic non-abelian anyons from conventional fractional quantum hall states, *Nature Communications* **4**, 1348 EP (2013), article.
- [22] J. Alicea and P. Fendley, Topological phases with parafermions: Theory and blueprints, *Annual Review of Condensed Matter Physics* **7**, 119 (2016), <https://doi.org/10.1146/annurev-conmatphys-031115-011336>.
- [23] J. Klinovaja and D. Loss, Time-reversal invariant parafermions in interacting rashba nanowires, *Phys. Rev. B* **90**, 045118 (2014).
- [24] L. H. Santos and T. L. Hughes, Parafermionic wires at the interface of chiral topological states, *Phys. Rev. Lett.* **118**, 136801 (2017).
- [25] J. Klinovaja, A. Yacoby, and D. Loss, Kramers pairs of majorana fermions and parafermions in fractional topological insulators, *Phys. Rev. B* **90**, 155447 (2014).
- [26] D. Rossini, M. Carrega, M. Calvanese Strinati, and L. Mazza, Anyonic tight-binding models of parafermions and of fractionalized fermions, *Phys. Rev. B* **99**, 085113 (2019).
- [27] A. Chew, D. F. Mross, and J. Alicea, Fermionized parafermions and symmetry-enriched majorana modes, *Phys. Rev. B* **98**, 085143 (2018).
- [28] A. Alexandradinata, N. Regnault, C. Fang, M. J. Gilbert, and B. A. Bernevig, Parafermionic phases with symmetry breaking and topological order, *Phys. Rev. B* **94**, 125103 (2016).
- [29] A. Calzona, T. Meng, M. Sassetti, and T. L. Schmidt, F_4 parafermions in one-dimensional fermionic lattices, *Phys. Rev. B* **98**, 201110(R) (2018).
- [30] E. Vernek, P. H. Penteado, A. C. Seridonio, and J. C. Egues, Subtle leakage of a majorana mode into a quantum dot, *Phys. Rev. B* **89**, 165314 (2014).
- [31] D. A. Ruiz-Tijerina, E. Vernek, L. G. G. V. Dias da Silva, and J. C. Egues, Interaction effects on a majorana zero mode leaking into a quantum dot, *Phys. Rev. B* **91**, 115435 (2015).
- [32] R. L. R. C. Teixeira and L. G. G. V. Dias da Silva, Quantum dots as parafermion detectors, *Phys. Rev. Research* **3**, 033014 (2021).
- [33] Y. Oreg, G. Refael, and F. von Oppen, Helical liquids and majorana bound states in quantum wires, *Phys. Rev. Lett.* **105**, 177002 (2010).
- [34] R. M. Lutchyn, J. D. Sau, and S. Das Sarma, Majorana fermions and a topological phase transition in semiconductor-superconductor heterostructures, *Phys. Rev. Lett.* **105**, 077001 (2010).
- [35] J. Alicea, New directions in the pursuit of majorana fermions in solid state systems, *Rep. Prog. Phys.* **75**, 076501 (2012).
- [36] U. Schollwöck, The density-matrix renormalization group, *Rev. Mod. Phys.* **77**, 259 (2005).

- [37] U. SchollwÄck, The density-matrix renormalization group in the age of matrix product states, *Annals of Physics* **326**, 96 (2011), january 2011 Special Issue.
- [38] M. Fishman, S. R. White, and E. M. Stoudenmire, The ITensor software library for tensor network calculations (2020), [arXiv:2007.14822](https://arxiv.org/abs/2007.14822).
- [39] C. D. Batista and G. Ortiz, Generalized jordan-wigner transformations, *Phys. Rev. Lett.* **86**, 1082 (2001).
- [40] Y. Zhuang, H. J. Changlani, N. M. Tubman, and T. L. Hughes, Phase diagram of the \mathbb{Z}_3 parafermionic chain with chiral interactions, *Phys. Rev. B* **92**, 035154 (2015).
- [41] F. Iemini, C. Mora, and L. Mazza, Topological phases of parafermions: A model with exactly solvable ground states, *Phys. Rev. Lett.* **118**, 170402 (2017).
- [42] S. R. White, Density-matrix algorithms for quantum renormalization groups, *Phys. Rev. B* **48**, 10345 (1993).
- [43] To compute the entanglement entropy, we perform DMRG calculations fully preserving the \mathbb{Z}_3 symmetry. The entanglement entropy is then calculated at the system’s center bond.
- [44] The exponential decay happens as long as μ is such that does not break the \mathbb{Z}_3 symmetry.
- [45] S. Das Sarma, J. D. Sau, and T. D. Stanescu, Splitting of the zero-bias conductance peak as smoking gun evidence for the existence of the majorana mode in a superconductor-semiconductor nanowire, *Phys. Rev. B* **86**, 220506(R) (2012).
- [46] Alternatively, the first summation over all powers of d guarantees that we can choose a “reference” state $|\varphi\rangle \equiv |0\rangle$ and sum only sum over $|\varphi'\rangle$, without the need to normalize by n_{gs} . For simulation purposes we used the ground state with Fock parafermion number 0 as “ $|0\rangle$ ”, however any other ground state yield the same result.
- [47] W. Li, A. Weichselbaum, and J. vonDelft, Identifying symmetry-protected topological order by entanglement entropy, *Phys. Rev. B* **88**, 245121 (2013).
- [48] E. Cobanera and G. Ortiz, Fock parafermions and self-dual representations of the braid group, *Phys. Rev. A* **89**, 012328 (2014).
- [49] The problem arises in the \mathbb{Z}_3 case mainly because there is no single fermionic operator connecting the up and down states. By contrast, in the case of \mathbb{Z}_4 parafermions, two sequential FPF numbers are connected by a single fermionic operator, eliminating the problem.